Systematic design of a magneto-rheological fluid embedded pneumatic vibration isolator subject to practical constraints

2012 Smart Mater. Struct. 21 035006

(http://iopscience.iop.org/0964-1726/21/3/035006)

Smart Mater. Struct. **21** (2012) 035006 (15pp) doi:10.1088/0964-1726/21/3/035006

Systematic design of a magneto-rheological fluid embedded pneumatic vibration isolator subject to practical constraints

Xiaocong Zhu, Xingjian Jing[1] and Li Cheng

Department of Mechanical Engineering, Hong Kong Polytechnic University, Hung Hom, Kowloon, Hong Kong, People's Republic of China

E-mail: xingjian.jing@polyu.edu.hk

Received 25 October 2011, in final form 26 December 2011
Published 2 February 2012
Online at stacks.iop.org/SMS/21/035006

Abstract
A systematic design of a magneto-rheological fluid embedded pneumatic vibration isolator (MrEPI) considering practical constraints and optimal performance is proposed. The design procedure basically consists of three steps, i.e. system level design, component level design and practical realization. The system level design involves synthesizing appropriate non-dimensional system parameters of pneumatic spring and MR damper elements based on parameter sensitivity analysis considering requirements for compact and efficient hardware utilization. The component level design involves optimal design of the MR valve by minimizing an objective function in terms of non-dimensional geometric, material and excitation parameters, and guaranteeing required performance in the worst cases. Then practical realization involves determining actual plant parameters from the non-dimensional analysis in system and component level designs with the considerations of practical requirements/constraints. To verify the effectiveness of this optimization procedure, the semi-active vibration control performance of the optimized MrEPI subject to harmonic disturbances is evaluated, which shows good isolation performance in all tested cases. This study actually provides a systematic method for the optimal analysis and design of all those nonlinear vibration isolators consisting of pneumatic spring and MR damper elements. This is achieved firstly by developing effective sensitivity analysis of dominant design parameters upon the adjustable stiffness and damping capacity irrespective of bulky or small system mass configuration and subsequently via a systematic realization design with the consideration of practical constraints in applications.

(Some figures may appear in colour only in the online journal)

1. Introduction

Vibration isolators are usually installed between the support foundation and equipment to prevent sensitive equipment from environmental vibration and impact shock as well as force disturbance. Typical applications include vehicle suspensions, air craft landing gears, optical tables, seismic protection etc [1–6, 31]. Compared with passive vibration isolators, semi-active and active ones could achieve superior vibration isolation and suppression performance due to adjustable damping and/or stiffness and flexibility in force control. Importantly, it is more and more noted that a vibration isolator with independent control of stiffness and damping could have very promising advantages in various vehicle suspensions under different road requirements, advanced landing gear systems for soft and hard landings,

[1] Author to whom any correspondence should be addressed.

combined shock and vibration devices etc [1, 4, 7–11]. To this end, a novel magneto-rheological fluid embedded pneumatic vibration isolator (MrEPI) was developed in [12] for general vibration isolation applications. This system can be regarded as a generic nonlinear vibration isolator system, which is composed of pneumatic spring and MR damper elements with hybrid and compact connection. The MrEPI allows independently adjustable stiffness, damping and height control with considerable maneuverable range and exhibits advantages of compact structure, less sealing and low power consumption, flexible and versatile control modes [12]. The advantageous dynamic performance of the MrEPI has been demonstrated through developing a nonlinear non-dimensional dynamic model with full consideration of nonlinear pneumatic springs and MR dampers. The MrEPI could be a versatile and flexible tool in various applications for vibration suppression and control. From a system engineering point of view, it is rather important to have a systematic optimization method in analysis and design for the development of a MrEPI for a specific application. However, the optimal design of the MrEPI is very complex due to many design parameters that could be coupled together in the pneumatic cylinders and MR valve, which also result in the difficulty in analysis of achievable performance and relevant sensitivity. To address these problems, a systematic optimization procedure is proposed in this study based on the non-dimensional analysis of a generic MrEPI system (i.e. any vibration isolation system composed of pneumatic springs and MR dampers) in consideration of different application requirements but regardless of concrete load mass configuration.

There are several papers focusing on the optimal design of a dual-chamber pneumatic spring system, which is actually a part of the MrEPI. Specifically, Holtz and Niekerk proposed an air-spring coupled to an auxiliary volume optimized by auxiliary volume size and flow restriction diameters for different loads through a number of trial and error simulations [13]. Quaglia and Sorli presented the optimal design of a pneumatic suspension system with design parameters including ratio between natural pulsations (optimal damping), volumetric stiffness of spring and auxiliary chamber [14]. Lee and Kim proposed an efficient transmissibility design wherein a complex stiffness model for a dual-chamber pneumatic vibration isolator with three design parameters (the volume ratio between two pneumatic chambers, the geometry of the capillary tube connecting the two pneumatic chambers, the stiffness of the diaphragm employed for prevention of air leakage) [15]. Moon and Lee analyzed the sensitivity of the vibration isolation performance of a pneumatic vibration isolation system in two air chambers using a fractional derivative model for the diaphragm and a quadratic damping model for the air flow restrictor [16]. Maciejewski *et al* presented an optimal indirect system for achieving the best compromise between the conflicting vibro-isolation criteria [17]. It is noted that the optimal design of pneumatic isolators in the literature usually focuses on the orifice or capillary tube damping and volume ratio parameters of the dual-chamber. However, there are few comments about the optimal design of nonlinear ratio and pressure ratio in a nonlinear pneumatic vibrator, which could have an obvious influence on the achievable performance and other design factors such as compactness and sensitivity [12]. On the other hand, the optimal design of the MR valve, which is an important element in damping control of MR dampers (adopted by the MrEPI), has also been studied in the literature [3, 6, 18]. In existing results, a multi-objective function with weighted indices of the MR fluid damper/valve is employed. Then a typical optimization procedure involving design of mechanical geometric scales and electromagnetic circuits is conducted through using a sequential least squares method or ANSYS magnetic routines. In particular, the volume constrained optimization of the MR fluid control valve/damper was also investigated in recent years [19–25]. However, it is noted that the conventional multi-objective function utilized in the literature has unclear weight selections, and the parameter setting for the design process is usually specified from trial and error with no consideration of practical constraints according to real application requirements. The minimum damping ratio (off-state damping) that actually plays an important role in isolation performance at high frequency is rarely considered in the optimization procedure of a conventional optimal design of MR valves [26, 27]. Moreover, the quantitative performance variation with respect to multiple and coupling design parameters is seldom commented on due to the difficulty in analysis of complex fluid flow characteristics and magnetic flux distribution. Therefore, optimization methods for the design of MR valves to fulfil practical constraints and to have a systematic procedure for parameter determination are yet to be developed. All those issues discussed above will be addressed for the optimal design of a MrEPI system in this study.

The paper is organized as follows. Section 2 gives a simple introduction of the schematic structure and modeling of the MrEPI. The optimal design process of the MrEPI is presented in section 3, which includes the system level design of the pneumatic spring and MR damping, the component level design of the MR valve and the final practical realization. Section 4 demonstrates the achievable semi-active vibration performance for the MrEPI with the optimal design. A conclusion is given thereafter.

2. Schematic structure and modeling of the MrEPI

The schematic structure of the MrEPI is shown in figure 1. It consists of three low chambers filled with air gas (CG1, CG2, CG3) and two upper chambers filled with MR fluid (CM1, CM2). Chamber CG1 and Chamber CG2, functioning as a dual-working-chamber pneumatic spring to provide adjustable stiffness and height control, are separated by a moving piston with diaphragm seals and controlled by four pneumatic high speed on–off valves. An auxiliary chamber CG3 is connected to Chamber CG2 with a flow restrictor that is designed to operate on a laminar flow region for linear damping. An MR valve is connected to the two sides of a

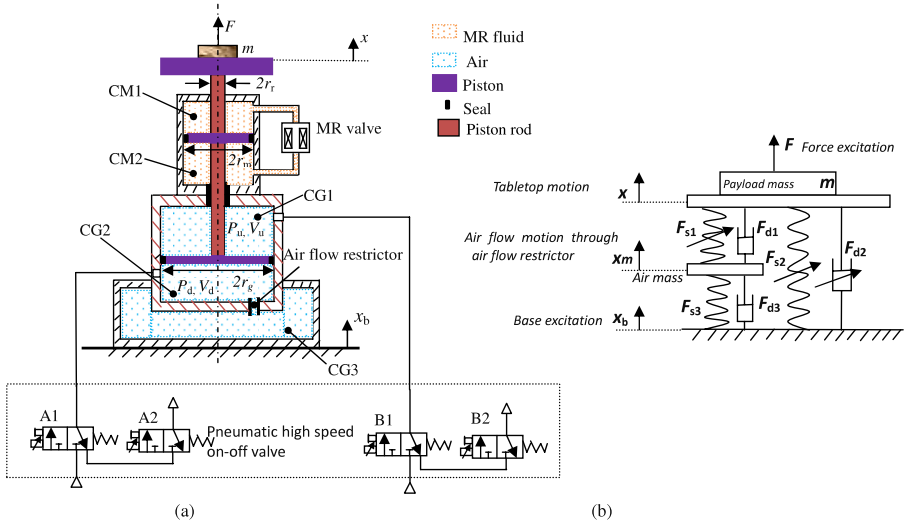

Figure 1. (a) The schematic structure of the MrEPI and (b) its equivalent mechanical system.

double-rod cylinder filled with MR fluids (Chamber CM1 and CM2) to provide adjustable damping.

The non-dimensional analytical models can be given by [12]:

$$\frac{\mathrm{d}^2\phi_x}{\mathrm{d}\phi_\mathrm{t}^2} = F_{\mathrm{snb1}}(\phi_x - \phi_{\mathrm{xm}}) - s_{\mathrm{u2}}F_{\mathrm{sna2}}(\phi_x - \Phi_{\mathrm{xb}}) - F_{\mathrm{dn2}}\left(\phi_x - \Phi_{\mathrm{xb}}, \frac{\mathrm{d}\phi_x}{\mathrm{d}\phi_\mathrm{t}} - \frac{\mathrm{d}\Phi_{\mathrm{xb}}}{\mathrm{d}\phi_\mathrm{t}}\right) + \Phi_F \quad (1)$$

$$F_{\mathrm{snb1}}(\phi_x - \phi_{\mathrm{xm}}) = F_{\mathrm{snb3}}(\phi_{\mathrm{xm}} - \Phi_{\mathrm{xb}}) - F_{\mathrm{dn3}}\left(\phi_{\mathrm{xm}} - \Phi_{\mathrm{xb}}, \frac{\mathrm{d}\phi_{\mathrm{xm}}}{\mathrm{d}\phi_\mathrm{t}} - \frac{\mathrm{d}\Phi_{\mathrm{xb}}}{\mathrm{d}\phi_\mathrm{t}}\right)$$

with the non-dimensional output force of the pneumatic spring element given by

$$F_{\mathrm{sn}i}(\phi_{\mathrm{xp}i}) = F_{\mathrm{snb}i}(\phi_{\mathrm{xp}i}) - s_{\mathrm{u}i}F_{\mathrm{sna}i}(\phi_{\mathrm{xp}i}) \quad (2a)$$

$$F_{\mathrm{snb}i}(\phi_{\mathrm{xp}i}) = \frac{\phi_\mathrm{L}}{\kappa}\left\{(1+\phi_{P0i})\left[\frac{\phi_\mathrm{L}(1+\phi_{V0i})}{\phi_\mathrm{L}(1+\phi_{V0i})+\phi_{\mathrm{xp}i}}\right]^{\kappa} - 1\right\}, \quad (2b)$$

$$F_{\mathrm{sna}i}(\phi_{\mathrm{xp}i}) = \phi_{KPi}\frac{\phi_\mathrm{L}}{\kappa}\left[\frac{\phi_{KLi}\phi_\mathrm{L}(1+\phi_{V0i})}{\phi_{KLi}\phi_\mathrm{L}(1+\phi_{V0i})-\phi_{\mathrm{xp}i}}\right]^{\kappa} \quad (2c)$$

where F_{sna} is the non-dimensional output force of the pneumatic spring due to the upper chamber, F_{snb} is the non-dimensional output force of the pneumatic spring due to the lower chamber and the non-dimensional output force of the MR damper element is given by

$$F_{\mathrm{dn}i}(\phi_{\mathrm{xp}i}, \dot{\phi}_{\mathrm{xp}i}) = F_{\mathrm{dna}i}(\dot{\phi}_{\mathrm{xp}i}) + F_{\mathrm{dnp}i}(\phi_{\mathrm{xp}i}, \dot{\phi}_{\mathrm{xp}i}) \quad (3a)$$

$$F_{\mathrm{dna}i}(\phi_{\mathrm{xp}i}, \dot{\phi}_{\mathrm{xp}i}) = 2\xi_i\phi_{\mathrm{DVMR}i}\tanh[(\dot{\phi}_{\mathrm{xp}i} + \phi_{\lambda ai}\phi_{\mathrm{xp}i})\phi_{\lambda bi}], \quad (3b)$$

$$F_{\mathrm{dnp}i} = 2\xi_i\dot{\phi}_{\mathrm{xp}i} \quad (3c)$$

where F_{dna} is the non-dimensional active damping force of the MR damper element and F_{dnp} is the non-dimensional passive damping force of the MR damper element.

The base excitation can be described by

$$\Phi_{x\mathrm{b}} = \sin(\Omega\phi_\mathrm{t} + \varphi) \qquad \frac{\mathrm{d}\Phi_{x\mathrm{b}}}{\mathrm{d}\phi_\mathrm{t}} = \phi_\omega\cos(\Omega\phi_\mathrm{t} + \varphi) \quad (4)$$

and the force excitation by

$$\Phi_F = \sin(\Omega\phi_\mathrm{t} + \varphi) \quad (5)$$

where ϕ_x, Ω, ϕ_t, φ are the non-dimensional absolute displacement of payload, excitation angular frequency, time and phase respectively. $\phi_{\mathrm{xp}i}$ is the relative displacement. ϕ_L, ϕ_{V0i}, ϕ_{P0i}, ϕ_{KPi} and ϕ_{KLi} are the non-dimensional adjustable variables related to each pneumatic spring element. ξ_i, $\phi_{\mathrm{DVMR}i}$, $\phi_{\lambda\mathrm{a}i}$, $\phi_{\lambda\mathrm{b}i}$ are non-dimensional variables related to each MR damper element (including passive viscous damping). The subscript $i = 1$–3 represents the components consisting of pneumatic spring and MR damper elements. The detailed definitions and illustrations of these variables are given in the appendix to this paper.

It can be seen that the MrEPI employs a hybrid configuration of two pneumatic elements in series connection and one MR damper element in parallel. The system can have a relatively compact structure, achieve independently adjustable stiffness (that is produced by pressure/volume regulation of pneumatic chambers using on–off valves) and damping (that is produced by current regulation of the MR valve) characteristics of considerably large maneuverable ranges and thus theoretically exhibit excellent isolation performance (e.g. small resonance peak values and high capability of resisting force disturbance as well as fast decaying rate at high frequencies under certain stiffness). It can provide the flexibility in switching between different working modes (e.g. passive control realized by closing all pneumatic on–off valves and applying zero current to the MR valve, semi-active control realized by pressure/volume regulation of the pneumatic chamber and current adjustment of the MR valve, and active control realized by arbitrary actuator force regulation of the pneumatic chamber), have

independent height control within a large range, produce high output force and will be convenient in manipulation with lower power and sealing requirements [12].

3. Design of the MrEPI considering practical constraints and high efficiency

A systematic design procedure for the MrEPI considering practical constraints and high efficiency will be established: (a) the system level design is to achieve performance as much as possible with compact and efficient hardware utilization through appropriately specifying non-dimensional design parameters of pneumatic springs and MR dampers; (b) the component level design is to provide optimal non-dimensional parameters of the MR valve through employing an objective function with predefined threshold for guaranteeing the required worst performance from system level design; (c) finally, the practical realization is used to obtain actual plant parameters according to practical application requirements.

3.1. System level design

From equation (1), some non-dimensional parameters should be tentatively synthesized for obtaining achievable isolation performance of the MrEPI as much as possible, which includes nonlinear ratio ϕ_{L}, additional volume ratio ϕ_{V01}, additional pressure ratio ϕ_{P01} and damping ratio of air restrictor ξ_3 for characterizing achievable stiffness related to the natural frequency of the system, and passive damping ratio ξ_2 and dynamic range ϕ_{DVMR} for characterizing achievable damping performances.

3.1.1. Natural frequency of the system. The output force of the MrEPI under harmonic piston motion is given according to equation (1)

$$\begin{aligned} F_{\mathrm{n}}(\Omega) &= F_{\mathrm{snb1}}(\phi_x - \phi_{x\mathrm{m}}) - s_{\mathrm{u}2}F_{\mathrm{sna2}}(\phi_x - \Phi_{x\mathrm{b}}) \\ &\quad - F_{\mathrm{dn2}}(\phi_x - \Phi_{x\mathrm{b}}, \mathrm{j}\Omega(\phi_x - \Phi_{x\mathrm{b}})) \\ F_{\mathrm{snb1}}(\phi_x - \phi_{x\mathrm{m}}) &= F_{\mathrm{snb3}}(\phi_{x\mathrm{m}} - \Phi_{x\mathrm{b}}) \\ &\quad - F_{\mathrm{dn3}}(\phi_{x\mathrm{m}} - \Phi_{x\mathrm{b}}, \mathrm{j}\Omega(\phi_{x\mathrm{m}} - \Phi_{x\mathrm{b}})). \end{aligned} \tag{6}$$

After linearization by substituting equations (2) and (3) into (6), the small variation of equation (6) is derived as

$$\begin{aligned} \delta F_{\mathrm{n}}(\Omega) &= -\frac{1+\phi_{P01}}{1+\phi_{V01}}[\delta\phi_x(\Omega) - \delta\phi_{\mathrm{m}}(\Omega)] \\ &\quad - s_{\mathrm{u}2}\phi_{KP2}\frac{1}{\phi_{KL2}(1+\phi_{V02})}[\delta\phi_x(\Omega) - \delta\Phi_{x\mathrm{b}}(\Omega)] \\ &\quad - \frac{1+\phi_{P01}}{1+\phi_{V01}}[\delta\phi_x(\Omega) - \delta\phi_{\mathrm{m}}(\Omega)] \\ &= -\frac{1+\phi_{P03}}{1+\phi_{V03}}[\delta\phi_{x\mathrm{m}}(\Omega) - \delta\Phi_{x\mathrm{b}}(\Omega)] \\ &\quad - 2\xi_3\mathrm{j}\Omega[\delta\phi_{x\mathrm{m}}(\Omega) - \delta\Phi_{x\mathrm{b}}(\Omega)]. \end{aligned} \tag{7}$$

Therefore, the small variation of non-dimensional spring force is given by

$$\begin{aligned} &\delta F_{\mathrm{n}}(\Omega) \\ &= -\left[\frac{1+\phi_{P01}+2\xi_3\,\mathrm{j}\Omega(1+\phi_{V03})}{2+\phi_{V01}+\phi_{V03}+2\xi_3\,\mathrm{j}\Omega(1+\phi_{V01})(1+\phi_{V03})}\right. \\ &\quad \left. + \frac{s_{\mathrm{u}2}\phi_{KP2}}{\phi_{KL2}(1+\phi_{V02})}\right][\phi_x(\Omega) - \Phi_{x\mathrm{b}}(\Omega)]. \end{aligned} \tag{8}$$

Thus, the linearized complex equivalent stiffness of the entire system with hybrid connection of pneumatic spring elements (component 1 and component 3 are connected in series, and the whole is connected with component 2 in parallel) is then given as follows, which is used to quantitatively characterize the viscoelastic behavior of the isolator.

$$\begin{aligned} K^* &= -\frac{\delta F_{\mathrm{n}}}{\delta[\phi_x(\Omega) - \Phi_{x\mathrm{b}}(\Omega)]} \\ &= \left[\frac{1+\phi_{P01}+2\xi_3\,\mathrm{j}\Omega(1+\phi_{V03})}{2+\phi_{V01}+\phi_{V03}+2\xi_3\,\mathrm{j}\Omega(1+\phi_{V01})(1+\phi_{V03})}\right. \\ &\quad \left. + \frac{s_{\mathrm{u}2}\phi_{KP2}}{\phi_{KL2}(1+\phi_{V02})}\right]. \end{aligned} \tag{9}$$

The linearized equivalent spring stiffness and loss stiffness is derived from equation (9) with $K^* = K_{\mathrm{equ}} + \mathrm{j}K_{\mathrm{lost}}$

$$\begin{aligned} K_{\mathrm{equ}} &= \{(1+\phi_{P01})^3(2+\phi_{V01}+\phi_{V03}) + 4\xi_3^2(1+\phi_{P01}) \\ &\quad \times (1+\phi_{V01})\,(1+\phi_{V03})^2\,\Omega^2\}\{(1+\phi_{P01})^2 \\ &\quad \times (2+\phi_{V01}+\phi_{V03})^2 + 4\xi_3^2\,(1+\phi_{V01})^2 \\ &\quad \times (1+\phi_{V03})^2\,\Omega^2\}^{-1} + \frac{s_{\mathrm{u}2}\phi_{KP2}}{\phi_{KL2}(1+\phi_{V02})} \end{aligned} \tag{10a}$$

$$\begin{aligned} K_{\mathrm{lost}} &= \{(1+\phi_{V01})^2(1+\phi_{V03})(2+\phi_{V01}+\phi_{V03}) \\ &\quad - (1+\phi_{\mathrm{p}01})(1+\phi_{V01})(1+\phi_{V03})\} \\ &\quad \times \{(1+\phi_{V01})^2\,(2+\phi_{V01}+\phi_{V03})^2 \\ &\quad + 4\xi_3^2\,(1+\phi_{V01})^2\,(1+\phi_{V03})^2\,\Omega^2\}^{-1}2\xi_3\Omega. \end{aligned} \tag{10b}$$

In the above analysis, the nonlinear ratio ϕ_{L} is not included in the formulation of the complex stiffness due to the linearization approximation. For a more accurate evaluation of the complex stiffness incurred by nonlinear ratio ϕ_{L}, the nonlinear complex stiffness composed of K'_{equ} and K'_{lost} could alternatively be calculated by equation (12) with an assumption that the isolator system is subject to harmonic displacement excitation $x(\phi_{\mathrm{t}})$ and the viscoelastic force $f(\phi_{\mathrm{t}})$ from $F_{\mathrm{n}}(\Omega)$ is calculated through a Fourier series [28]. The linear complex stiffness and nonlinear complex stiffness will be employed for determining the appropriate configuration of ϕ_{L} and ξ_3 later.

$$K'_{\mathrm{equ}} = \frac{F_{\mathrm{c}}X_{\mathrm{c}} + F_{\mathrm{s}}X_{\mathrm{s}}}{X_{\mathrm{c}}^2 + X_{\mathrm{s}}^2}, \tag{11a}$$

$$K'_{\mathrm{lost}} = \frac{F_{\mathrm{c}}X_{\mathrm{s}} - F_{\mathrm{s}}X_{\mathrm{c}}}{X_{\mathrm{c}}^2 + X_{\mathrm{s}}^2} \tag{11b}$$

where $x(\phi_{\mathrm{t}}) = X_{\mathrm{c}}\cos\Omega\phi_{\mathrm{t}} + X_{\mathrm{s}}\sin\Omega\phi_{\mathrm{t}}, f(\phi_{\mathrm{t}}) = F_{\mathrm{c}}\cos\Omega\phi_{\mathrm{t}} + F_{\mathrm{s}}\sin\Omega\phi_{\mathrm{t}}$ and the loss factor and equivalent damping are

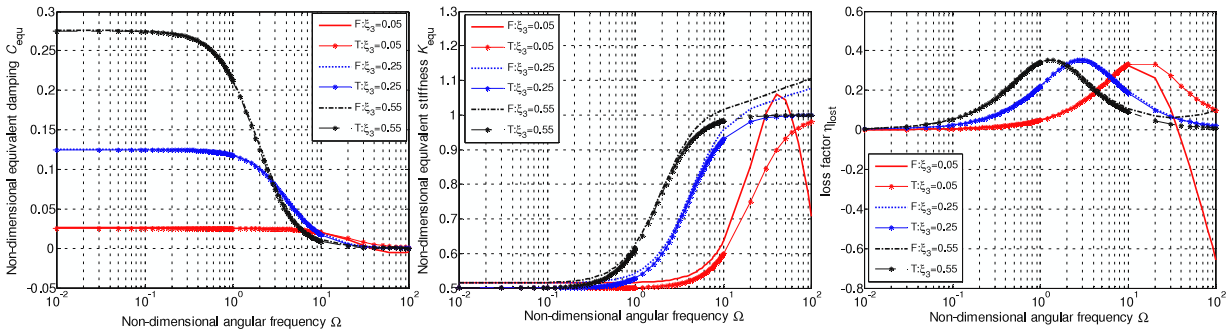

Figure 2. Quasi-steady performance of the MrEPI under different ξ_3 with the same $\phi_L = 3$. (Note: T represents the linear value calculated from equation (10) and F represents the nonlinear value calculated from equation (11).)

respectively calculated by [28]

$$\eta_{\text{lost}} = \frac{K_{\text{lost}}}{K_{\text{equ}}}, \tag{12a}$$

$$C_{\text{equ}} = \frac{K_{\text{lost}}}{\Omega}. \tag{12b}$$

Subsequently, the non-dimensional natural angular frequency is approximately given by

$$\begin{aligned}\Omega_{\text{n}} = \frac{\omega_{\text{n}}}{\omega_{\text{n0}}} = \sqrt{K_{\text{equ}}} = \{&\{(1+\phi_{P01})^3(2+\phi_{V01}+\phi_{V03}) \\ &+ 4\xi_3^2(1+\phi_{P01})(1+\phi_{V01})\,(1+\phi_{V03})^2\,\Omega^2\} \\ &\times \{(1+\phi_{P01})^2\,(2+\phi_{V01}+\phi_{V03})^2 \\ &+ 4\xi_3^2\,(1+\phi_{V01})^2\,(1+\phi_{V03})^2\,\Omega^2\}^{-1} \\ &+ \{s_{\text{u2}}\phi_{KP2}\}\,\{\phi_{KL2}(1+\phi_{V02})\}^{-1}\,\}^{1/2}. \end{aligned} \tag{13}$$

With the reference natural angular frequency defined as

$$\begin{aligned}\omega_{\text{n0}} &= \sqrt{\frac{k_0}{m_0}} = \sqrt{\frac{\kappa P_{\text{d0}} A_{\text{d}}}{m_0}} = \sqrt{\frac{\kappa(m_0 g + P_{\text{atm}} A_{\text{d}})}{L_0 m_0}} \\ &\approx \sqrt{\frac{\kappa g}{L_0}} \end{aligned} \tag{14}$$

where k_0 is the reference stiffness, m_0 is the reference mass load, P_{d0} is the initial pressure of the lower pneumatic chamber. A_{d} is the effective piston area of the lower pneumatic chamber. P_{atm} is the atmospheric pressure. L_0 is the initial length of the pneumatic chamber.

The adjustable stiffness related to the natural frequency for fulfilling different application requirements depends on several non-dimensional parameters ϕ_{V01}, ϕ_{V02}, ϕ_{V03}, ϕ_{P01}, ξ_3, ϕ_{KP2}, ϕ_{KL2}. Note that $\phi_{P01} = \phi_{P03} = \phi_{KP2}$ is established under invariant static displacement, and $\phi_{V02} = 0$, $\phi_{KL2} = 1$ are used for convenience in design. In the following, the performance incurred by ϕ_{V01}, ϕ_{P01}, ξ_3 and ϕ_{L} will be analyzed and the parameter selection will be discussed.

3.1.2. Specification of ϕ_L and ξ_3 for the pneumatic spring. The required volume of the pneumatic chamber is strongly dependent on the nonlinear ratio ϕ_{L} since the total volume is calculated as $V_{\text{t}} = \phi_{\text{L}}\hat{x}_{\text{b0}}[3 + \phi_{V01} + \phi_{V03}]$ in which $\hat{x}_{\text{b0}}$ is the maximum excitation amplitude. Therefore, it is possible to employ small ϕ_{L} for compact isolator design. However, when ϕ_{L} is small, there is stronger unexpected nonlinear behavior such as super-harmonics in transmissibility, poorer force mobility and larger average displacement at resonance and high frequency. Fortunately, the unsatisfactory behavior could be improved through introducing the viscous damping between the lower chamber of the dual-working-chamber and the auxiliary chamber (ξ_3) for providing sufficient damping in the isolation system. Therefore, ϕ_{L} and ξ_3 should be designed first for meeting the requirement of small gas volume and better isolation performance as much as possible.

Figure 2 shows the comparison of linear and nonlinear quasi-static performance for the MrEPI under different ξ_3 with the same small ϕ_{L} ($\phi_{\text{L}} = 3$) and zero ξ_2. It can be seen from figure 2 that the equivalent damping is large at low frequency and small at high frequency, and the spring stiffness is small at low frequency and is increased at high frequency. The stringent variation occurs at frequencies near resonance frequency. The loss factor initially increases and then decreases when the excitation frequency is increasing. In particular, the loss factor is useful for evaluating resonance attenuation [15]. The linear loss factor is almost equal to the nonlinear loss factor only if ξ_3 is moderately specified ($\xi_3 \geq 0.25$) while an obvious difference happens for too small ξ_3, which will induce severe unexpected nonlinearity and excessive ξ_3 will deteriorate the isolation performance at high frequency. Therefore, an appropriate ξ_3 could be specified as $\xi_3 \approx 0.25$ for effectively removing unexpected nonlinear behavior of the pneumatic spring without violating the compact requirement in volume design (small ϕ_{L}).

Figures 3 and 4 show the quasi-static performance and dynamic isolation performance of the MrEPI under different ϕ_{L} and the same ξ_3. It can be seen from figure 3 that the equivalent damping and loss factor exhibit almost the same characteristics while the equivalent spring stiffness demonstrates a small difference for the MrEPI under different ϕ_{L} with appropriate ξ_3, which indicates that the nonlinear ratio ϕ_{L} could be set fairly small to make the stiffness slightly larger without significantly deteriorating resonance attenuation if ξ_3 can also be set appropriately. Similarly, it can be seen from figure 4 that the transmissibility of the MrEPI is almost the same while the force mobility shows a slight difference under different ϕ_{L} but with the same ξ_3. This is consistent with the result of quasi-static performance, i.e. the stiffness of the

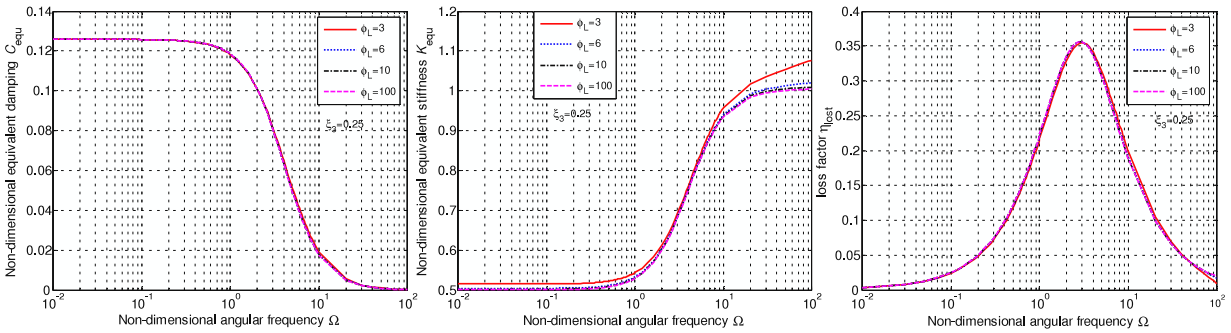

Figure 3. Quasi-steady performance of the MrEPI under different ϕ_L and the same ξ_3.

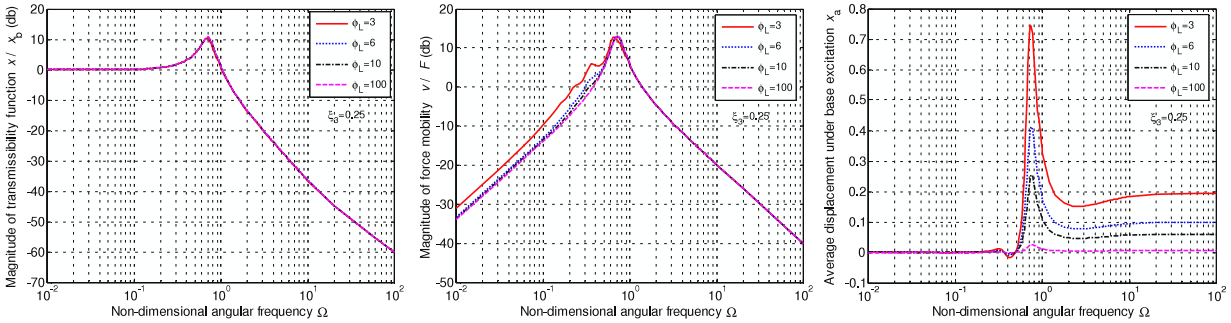

Figure 4. Isolation performance of the MrEPI under different ϕ_L and the same ξ_3.

system is slightly affected by ϕ_L and the transmissibility peak can be greatly decreased through appropriately choosing ξ_3 but irrespective of ϕ_L.

On the other hand, it is noted that the ratio of operational pressure over initial pressure (referred to as pressure variation ratio ε_p) of one pneumatic chamber is strongly dependent on ϕ_L shown as equation (15), which is derived from equations (1) and (2).

$$\left[\frac{1}{1+1/\phi_L}\right]^{\kappa} \leq \varepsilon_p = \frac{P_g}{P_0} \leq \left[\frac{1}{1-1/\phi_L}\right]^{\kappa}. \qquad (15)$$

Figure 5 shows the limitation of pressure variation ratio under harmonic excitation along with adjustable nonlinear ratio ϕ_L. It can be seen from figure 5 that the pressure variation ratio is significantly large under small ϕ_L and gradually decreases with ϕ_L increasing. It is appreciable that the pressure variation ratio should be as small as possible for achieving more adjustable stiffness due to pressure variation, and that ϕ_L should be as small as possible for compact design due to decreased volume size. Therefore, it is appropriate to specify the nonlinear ratio to be $\phi_L = 3$–6 with the pressure variation ratio being $0.732 \leq \varepsilon_p \leq 1.5$ for compromising the compact design and small pressure variation.

3.1.3. Specification of ϕ_{V01} for pneumatic spring. The additional volume ratio ϕ_{V01} is used to adjust the stiffness. According to equation (13), the relationship between the non-dimensional natural angular frequency Ω_n and the additional volume ratio ϕ_{V01} ($\phi_{P01} = 0$) is shown in figure 6. It can be seen from figure 6 that non-dimensional natural angular frequency is decreased rapidly with the additional

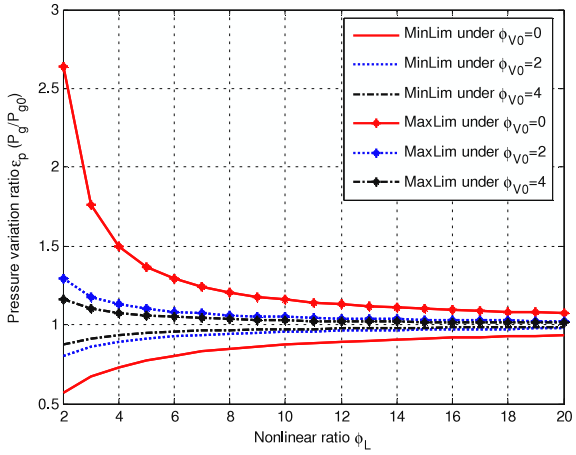

Figure 5. The limitation of pressure variation ratio during harmonic excitation under adjustable nonlinear ratio ϕ_L. (Note: 'MinLim' means 'minimum limitation of pressure variation ratio', 'MaxLim' means 'maximum limitation of pressure variation ratio'.)

volume ratio increasing but the decreasing rate becomes smaller for a larger ratio value. Thus, it is appropriate to choose $\phi_{V01} = 4$–5 since the variable non-dimensional natural angular frequency can be set down to 0.4 in this case and too large additional volume ratio has a slight influence on natural angular frequency.

3.1.4. Specification of ϕ_{P01} for the pneumatic spring.

(1) Permissible pressure ratio for variable stiffness adjustment. The additional pressure ratio ϕ_{P01} along with the

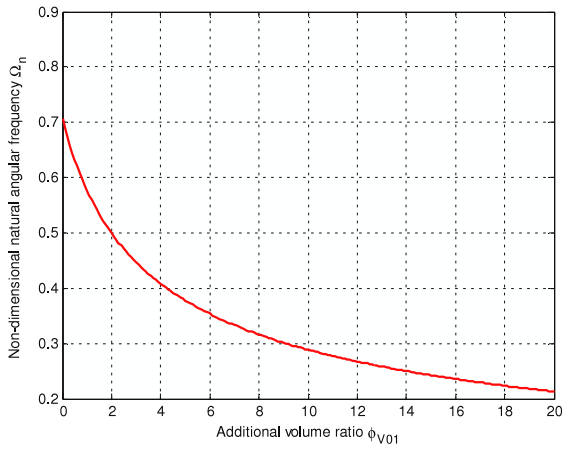

Figure 6. Relationship between natural angular frequency and additional volume ratio.

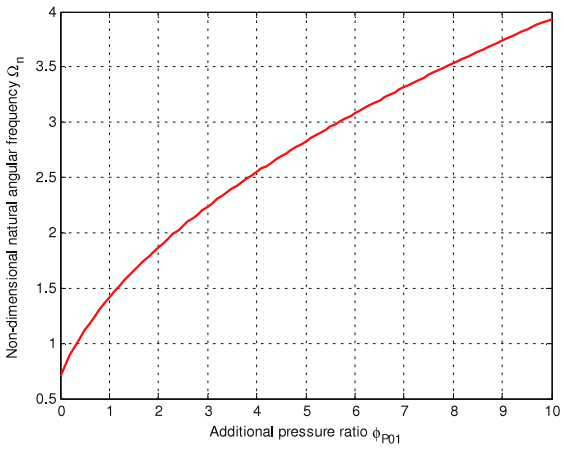

Figure 7. Relationship between natural angular frequency and additional pressure ratio.

same value of ϕ_{KP2} is utilized to adjust the stiffness of the system. According to equation (13), the relationship between the non-dimensional natural angular frequency and additional pressure ratio ϕ_{P01} ($\phi_{V01} = 0$) is shown in figure 7. The natural angular frequency is increased significantly when the additional pressure ratio increases but the slope becomes smaller for a larger additional pressure ratio value. Theoretically, additional pressure ratio ϕ_{P01} can be arbitrarily determined for adjustable stiffness of the system under the constraint of permissible source pressure of the system. In practice, it is preferable to employ $\phi_{P01} \leq 4$ for achieving both fairly large adjustable stiffness and keeping a moderate pressure variation for saving energy.

(2) Variable height adjustment. The additional pressure ratio ϕ_{P01} can also be utilized to adjust the isolator height (i.e. the static displacement) when ϕ_{P01} and ϕ_{KP2} are properly set [12]. The permissible variation of height is given by

$$-\alpha\phi_{\mathrm{L}} \leq \phi_{x\mathrm{p}0} = x_{\mathrm{p}0}/\hat{x}_{\mathrm{b}0} \leq \alpha\phi_{\mathrm{L}} \tag{16}$$

where α is a factor for the variable height range in view of the limitation of the piston stroke and $0 \leq \alpha \leq 1 - 1/\phi_{\mathrm{L}}$ is used for guaranteeing excitation space due to $\alpha\phi_{\mathrm{L}} \leq \phi_{\mathrm{L}} - 1$.

Supposing $\phi_{V01} = \phi_{V03} = 0$, the non-dimensional static displacement ϕ_x is given by equation (17) from equation (1)

$$(1+\phi_{P01})\left[\frac{1}{1+\frac{\phi_x-\Phi_{\mathrm{xb}}}{2\phi_{\mathrm{L}}}}\right]^{\kappa} - s_{\mathrm{u}2}\phi_{KP2}\left[\frac{1}{1-\frac{\phi_x-\Phi_{\mathrm{xb}}}{\phi_{KL2}\phi_{\mathrm{L}}}}\right]^{\kappa} = 1. \tag{17}$$

Then the required additional pressure ratio considering height limitation is given by equation (18) according to equations (16) and (17)

$$\left(1-\frac{\alpha}{2}\right)^{\kappa}\left[1+s_{\mathrm{u}2}\phi_{KP2}\left(\frac{1}{1+\alpha/\phi_{KL2}}\right)^{\kappa}\right] - 1 \leq \phi_{P01} \leq \left(1+\frac{\alpha}{2}\right)^{\kappa}\left[1+s_{\mathrm{u}2}\phi_{KP2}\left(\frac{1}{1-\alpha/\phi_{KL2}}\right)^{\kappa}\right] - 1. \tag{18}$$

The required additional pressure ratio for maximum/minimum height limitations is dependent on the nonlinear ratio ϕ_{L} if specifying $\alpha = 1 - 1/\phi_{\mathrm{L}}$. Figure 8 shows

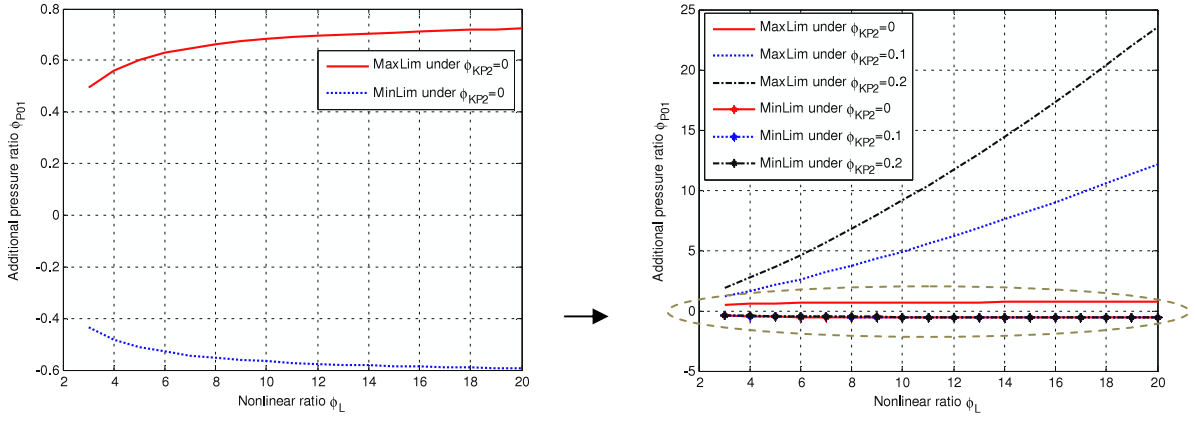

(a) (b)

Figure 8. The required pressure ratio at maximum/minimum height limitations along with different ϕ_{L} under (a) $\phi_{KP2} = 0$ and (b) several sets of ϕ_{KP2}.

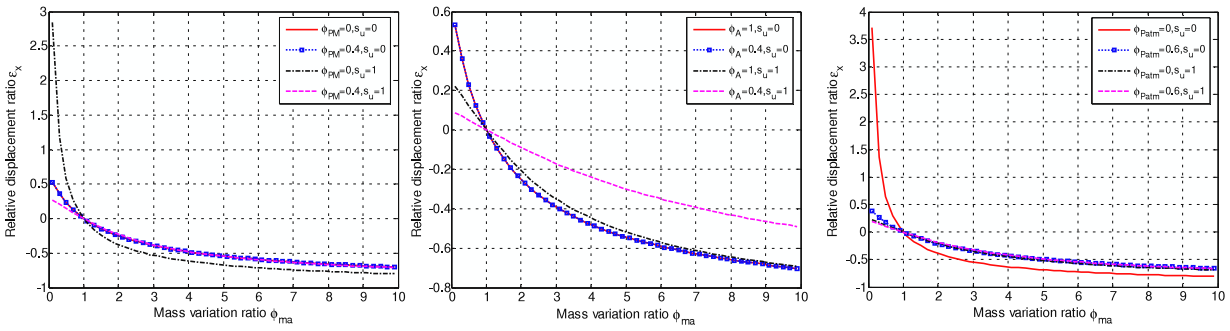

(a) (b) (c)

Figure 9. The relationship between relative displacement ratio and load mass variation ratio under (a) different basic load mass ratio ϕ_{PM}, (b) piston area ratio ϕ_A and (c) atmospheric pressure ratio $\phi_{P\text{atm}}$.

the required additional pressure ratio at maximum/minimum height limitations along with different nonlinear ratio ϕ_{L} under several sets of ϕ_{KP2}. It is seen from figure 8(a) that the required pressure ratio for maximum and minimum height is significantly dependent on small ϕ_{L} and slightly dependent on large ϕ_{L} for a single-working-chamber pneumatic spring ($\phi_{KP2} = 0$). The required pressure ratio for height limitation is usually not large (the required pressure ratio for the maximum height being less than 0.75 and for minimum height being larger than -0.6) at any ϕ_{L}, which indicates that the variable height adjustment with efficient utilization of air volume could be easily obtained in practical applications. On the other hand, figure 8(b) shows the required additional pressure ratio for the dual-working-pneumatic chamber utilized in MrEPI ($\phi_{KP2} \neq 0$). It is indicated that the required additional pressure ratio ϕ_{P01} for maximum height is greatly increased with ϕ_{KP2} while the required additional pressure ratio ϕ_{P01} for minimum height is slightly increased with ϕ_{KP2}, which implies that the maximum height for full space utilization of the dual-working-chamber with large initial volume is difficult to achieve due to the resistance effect of counter pressure in height control. Noticeably, ϕ_{P01} and ϕ_{KP2} for variable height control are usually not larger than the permissible ϕ_{P01} for variable stiffness control in the case of compact design (small ϕ_{L}).

(3) Permissible load mass. The static equilibrium equation is given by

$$A_{\text{d}}P_{\text{d0}} - s_{\text{u}}A_{\text{u}}P_{\text{u0}} = mg + P_{\text{atm}}A_{\text{d}} - s_{\text{u}}P_{\text{atm}}A_{\text{u}} \qquad (19)$$

where m is the load mass; A_{d}, A_{u} are the effective cross-sectional area of the lower and upper pneumatic chambers, respectively; P_{d0}, P_{u0} are the pressures of the lower and upper pneumatic chambers, respectively.

If the load mass is changed by Δm, the new static equilibrium equation is given by

$$A_{\text{d}}P_{\text{d}} - s_{\text{u}}A_{\text{u}}P_{\text{u}} = (m + \Delta m)g + P_{\text{atm}}A_{\text{d}} - s_{\text{u}}P_{\text{atm}}A_{\text{u}} \quad (20)$$

where $P_{\text{d}} = P_{\text{d0}}\left(\frac{V_{\text{d0}}}{V_{\text{d0}}+A_{\text{d}}x_{\text{p}}}\right)^{\kappa}$, $P_{\text{u}} = P_{\text{u0}}\left(\frac{V_{\text{u0}}}{V_{\text{u0}}-A_{\text{u}}x_{\text{p}}}\right)^{\kappa}$.

The load mass variation ratio ϕ_{ma} and the resulting non-dimensional static displacement ratio $\phi_{x\text{p0}}$ have the following relationship, in which the variable m from equation (19) and $m + \Delta m$ from equation (20) are combined together

$$\left(\frac{1}{1+\phi_{x\text{p0}}/\phi_{\text{L}}}\right)^{\kappa} - \phi_{\text{ma}} - s_{\text{u}}\phi_{PM}\left[\left(\frac{1}{1-\phi_{x\text{p0}}/(\phi_{KL}\phi_{\text{L}})}\right)^{\kappa} - \phi_{\text{ma}}\right] - \phi_{P\text{atm}}(1-\phi_{\text{ma}}) + s_{\text{u}}\phi_{P\text{atm}}\phi_A(1-\phi_{\text{ma}}) = 0 \qquad (21)$$

where $\phi_{\text{ma}} = \frac{\Delta m+m}{m}$, $\phi_{x\text{p0}} = \frac{x_{\text{p0}}}{x_{\text{b0}}}$, $\phi_{PM} = \frac{P_{\text{u0}}A_{\text{u}}}{P_{\text{d0}}A_{\text{d}}}$, $\phi_{KL} = \frac{L_{\text{u0}}}{L_{\text{d0}}}$, $\phi_A = \frac{A_{\text{u}}}{A_{\text{d}}}$, $\phi_{P\text{atm}} = \frac{P_{\text{atm}}}{P_{\text{d0}}}$, $L_{\text{d0}} = V_{\text{d0}}/A_{\text{d}}$, $L_{\text{u0}} = V_{\text{u0}}/A_{\text{u}}$.

The relative displacement ratio defined by $\varepsilon_x = \phi_{x\text{p0}}/\phi_{\text{L}}$ under different load mass variation ratio ϕ_{ma} is influenced by working mode s_{u}, atmosphere pressure ratio $\phi_{P\text{atm}}$, piston area ratio ϕ_A and basic load mass ratio ϕ_{PM}. Figure 9 shows the relationship between ε_x and ϕ_{ma} under different basic load mass ϕ_{PM}, piston area ratio ϕ_A and atmosphere pressure ratio $\phi_{P\text{atm}}$ with default values $s_{\text{u}} = 0$, $\phi_{PM} = 0.5$, $\phi_A = 0.9$, $\phi_{P\text{atm}} = 0.5$. It can be seen from figures 9(a) and (b) that ϕ_{PM} and ϕ_A have almost no influence on single-working-chamber mode and have significant influence upon the dual-working-chamber; an increase in ϕ_{PM} brings about a small increase in ε_x and an increase in ϕ_A a decrease of ε_x in the case of compression status (e.g. $\phi_{\text{ma}} > 1$). From figure 9(c), $\phi_{P\text{atm}}$ has obvious influence upon the relative displacement ratio of the single-working-chamber and slight influence upon the relative displacement ratio of the dual-working-chamber. It is especially noted from figure 9 that the influences incurred by all the parameters are usually larger with respect to smaller mass variation (e.g. $\varepsilon_x = 2.8$ when $\phi_{\text{ma}} = 0.1$) but smaller with larger mass variation (e.g. $\varepsilon_x = -0.8$ when $\phi_{\text{ma}} = 10$) under small ϕ_{PM} and small $\phi_{P\text{atm}}$. This indicates that better anti-disturbance performance suffering compression load could be achieved due to increased stiffness (which can be achieved by increased pressure). In practical application, the MrEPI can support a mass variation of up to five times with a relative displacement ratio at -0.6 for sufficient excitation stroke.

3.1.5. Specification of ξ_2 and ϕ_{DVMR} for the MR damper element. The semi-active damping control is utilized to attenuate the resonance peak and mitigate vibration energy.

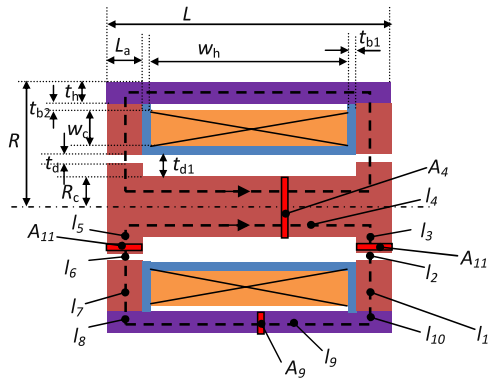

Figure 10. The schematic structure of the MR valve used in the MrEPI.

According to the non-dimensional dynamic model for the MR damper element, four important design parameters (e.g. passive damping ratio, dynamic range, hysteresis width coefficient and hysteresis slope coefficient) are used to characterize the performance of an MR valve [12].

It is noted that the transmissibility of the isolator at very high frequency is usually very small, therefore the isolation performance is generally evaluated within a frequency of 0–10Ω_n. On the one hand, small passive damping ratio ξ_2 is necessary for fast vibration mitigation in semi-active vibration control. It is demonstrated through simulations that the decaying rate of the transmissibility for the MrEPI within 0–10Ω_n is almost the same as the decaying rate using an ideal sky-hook for the semi-active isolator (-40 db) if $\xi_2 \leq 0.035$ is specified. Therefore, the passive damping ratio ξ_2 can be determined as less than 0.035 for guaranteeing fast vibration mitigation at high frequency. On the other hand, it is shown in the simulations that the dynamic range ϕ_{DVMR} should be as large as possible with a small passive damping ratio for achieving good performance (e.g. the good isolation performance is obtained with $\phi_{DVMR} \geq 50$, $\xi_2 \leq 0.05$ under $\phi_{P01} = 3$). That is, a large active damping force is needed for resonance attenuation in view of the proportional relationship between non-dimensional active damping and $2\xi_2\phi_{DVMR}$ from the non-dimensional dynamics of the MrEPI (equations (1)–(3)). Moreover, large hysteresis slope coefficient and small hysteresis width coefficient should be used for less hysteresis behavior existing in isolation control as indicated in [12], which implies that the time constant of the MR valve should be designed as small as possible to facilitate dynamic control [20].

3.2. Component level design

The component level design is conducted to determine the optimal geometric and material configuration of the MR valve based on the parameter requirements (e.g. required small passive damping ratio, time constant and maximizing dynamic range) from system level design.

3.2.1. Schematic structure and analytical model of the MR valve. The schematic structure of the MR valve with annular resistance flow channel used for the MrEPI is shown in figure 10, which has a slight difference from the conventional MR valve structure in view of the coil configuration [23]. Namely, the electromagnetic coil wound around a nonmagnetic coil bobbin is placed between the magnetic outer housing and the magnetic valve core, resulting in the annular duct between the magnetic pole and valve core with the advantages of easy wire protection due to the separation of coil wires and MR fluids. Note that the generic MR valve can either be placed outside of the cylinder in a bypass configuration or integrated in a moving piston inside the cylinder.

The damping force of the MR valve is given by [12, 29]

$$F_d(x_p, \dot{x}_p) = c_{vis}\dot{x}_p + (F_\tau + F_f)\tanh[(\dot{x}_p + \lambda_a x_p)\lambda_b] \qquad (22)$$

where x_p and $\dot{x}_p$ are the displacement and velocity of the piston respectively; F_τ is the yield force due to the MR effect with $F_\tau = \Delta P A_p = \frac{2nf_c\tau_y(H_{MR})L_a A_p}{t_d}$; ΔP is the pressure drop of the MR valve, A_p is the cross-sectional area of the piston in the MR damper cylinder with $A_p = \pi(r_1^2 - r_2^2) = \pi r^2$, r_1 and r_2 are the radii of the piston head and rod of the MR damper respectively; F_f is the friction force due to shaft seals; $F_\eta = C_{vis}\dot{x}_p$ is the Newtonian viscous force with $F_\eta = c_{vis}\dot{x}_p = F_{\eta 1} + F_{\eta 2} + F_{\eta 3}$ in which $F_{\eta 1} = \frac{24n\eta L_a A_p^2 \dot{x}_p}{w t_d^3}$, $F_{\eta 2} = \frac{12n\eta L_{p1} A_p^2 \dot{x}_p}{w_1 t_{d1}^3}$, $F_{\eta 3} = \frac{8\eta L_t}{\pi r_t^4} A_p^2 \dot{x}_p$, η is the viscosity of the MR fluid, L_a is the active length of the magnetic pole, L_{p1} is the passive gap length of the bobbin shaft with $L_{p1} = L/n - 2L_a$, n is the coil number, L is the total length of the MR valve, $w = 2\pi\bar{R}_d$ is the circumference of the annulus of the MR valve, $\bar{R}_d$ is the inner radius of the annulus of the magnetic pole, $w_1 = 2\pi\bar{R}_{d1}$, $\bar{R}_{d1}$ is the inner radius of the annulus of the bobbin shaft, L_t is the total length of tubing, r_t is the radius of circular tubing, t_d is the gap of the annulus and $\tau_y(H_{MR})$ is the dynamic yield shear stress of the MR fluid, which is dependent on the applied magnetic intensity H_{MR} in the electromagnetic circuit; λ_a is a parameter to capture the shape of the hysteresis loop that depends on piston displacement and λ_b is a parameter to capture the shape of yield force; $f_c = 2.07 + \frac{12Q\eta}{12Q\eta + 0.4wt_d^2\tau_y}$ is a coefficient that depends on the flow velocity profile and is bound to the interval [2.07, 3.07], w_c is the coil width, w_h is the coil height.

3.2.2. Performance in terms of non-dimensional parameters. The damper capability could be evaluated by several performance indices such as dynamic range, passive damping ratio, time constant etc. It can be formulated in terms of input non-dimensional variables (table 1) according to analytical models as:

$$\begin{aligned}
\phi_{DVMR} &= \frac{F_\tau}{F_\eta} = \frac{f_c}{12(\Delta_{p1} + \Delta_{p2}/\phi_{La})}\frac{\phi_r}{\phi_{Apd}}\frac{\tau_y(H_{MR})}{\eta}\phi_{gr}\frac{r_0}{v_p} \\
\xi_2 &= \frac{c_{vis}}{2\sqrt{mk_0}} = 12\pi n(\Delta_{p1}\phi_{La} + \Delta_{p2})\frac{\phi_{Apd}}{\phi_r^2}\phi_{E1}\phi_{gr} \\
F_\tau &= \pi r^2 \Delta P = 2nf_c\frac{\tau_y(H_{MR})}{\phi_r}\phi_{La}\phi_{gr}^2\pi r_0^2 \\
T_{in} &= \Delta_5[(\Delta_{H1} + \phi_{M1})\phi_{La} - \Delta_{H2}\phi_{La}^2]\phi_{gr}^2\frac{r_0^2}{r_{w1}}
\end{aligned} \qquad (23)$$

Table 1. Definitions of input non-dimensional variables for the MR valve. (Note: B_{sat} is the saturation of the magnetic material used for the MR valve including valve core, magnetic pole, outer housing etc. H_{MRsat}, μ_{MR} are the saturated magnetic intensity and relative permeability of MR fluids, respectively. r_0 is the reference radius of the MR damper cylinder dependent on the effective piston area of the pneumatic chamber A_{d}, A_w is the cross-sectional area of the copper coil. A_{dw} is the cross-sectional area of the annular gap given by $A_{\text{dw}} = wt_{\text{d}}$, $\bar{d}_{\text{c}}$ is the average diameter of the coil, I is the applied current, $\mu_0 = 4\pi \times 10^{-7}$, $v_{\text{p}} = \dot{x}_{\text{b0}}\omega_{\text{n0}}$ is the piston velocity.)

Non-dimensional variables	Definitions	
Geometry relevant variables	Normal geometry variable	$\phi_{\text{r}} = \frac{t_{\text{d}}}{r}$, $\phi_{\text{r1}} = \frac{R_{\text{c}}}{r}$, $\phi_{\text{r3}} = \frac{t_h}{r}$, $\phi_{\text{r4}} = \frac{R}{r}$, $\phi_{LP} = \frac{L}{r}$, $\phi_{\text{La}} = \frac{L_{\text{a}}}{r}$, $\phi_{\text{gr}} = \frac{r}{r_0}$
	Tubing geometry variable	$\phi_{pt} = \frac{L_{\text{t}}}{r}\frac{r^4}{r_{\text{t}}^4}$
	Additional geometry variable	$k_{\text{d}} = \frac{t_{\text{d1}}}{t_{\text{d}}}$, $k_{\text{b1}} = \frac{t_{\text{b1}}}{t_{\text{d}}}$, $k_{\text{b2}} = \frac{t_{\text{b2}}}{t_{\text{d}}}$
Material relevant variable		$\phi_{\text{M1}} = \frac{B_{\text{sat}}}{\mu_0\mu_{\text{MR}}H_{\text{MRsat}}}$
Exciting relevant variable		$\phi_{\text{M2}} = \frac{H_{\text{MRsat}}}{r_0 I/(2A_w)}$, $\phi_{\text{E1}} = \frac{\eta r_0}{m\omega_{\text{n0}}}$

where $\Delta_{\text{p1}} = 1 - \frac{1}{k_{\text{d}}^3}$, $\Delta_{\text{p2}} = \frac{\phi_{LP}}{2n}\frac{1}{k_{\text{d}}^3} + \frac{2}{3n}\phi_{pt}\phi_{\text{r}Rd}\phi_{\text{r}}^3$, $\phi_{Apd} = \frac{A_{\text{p}}}{A_{\text{dw}}} = \frac{1}{2\phi_{\text{r}Rd}\phi_{\text{r}}}$, $\Delta_5 = \mu_0\mu_{\text{MR}}\frac{\phi_{\text{r}Rd}}{\phi_{\text{r}dc}}$, $\Delta_{\text{H1}} = \frac{\phi_{\text{r}wc}}{\phi_{\text{r}}}[\frac{\phi_{LP}}{n} - 2k_{\text{b1}}\phi_{\text{r}}]$, $\Delta_{\text{H2}} = \frac{2\phi_{\text{r}wc}}{\phi_{\text{r}}}$, $\phi_{\text{r}Rd} = \frac{\bar{R}_{\text{d}}}{r} = \phi_{\text{r4}} - \phi_{\text{r3}} - \frac{1}{2}\phi_{\text{r}} - (\phi_{\text{r}wc} + k_{\text{b1}}\phi_{\text{r}} + k_{\text{b2}}\phi_{\text{r}})$, $\phi_{\text{r}dc} = \frac{\bar{d}_{\text{c}}}{r} = 2\phi_{\text{r1}} + \phi_{\text{r}wc} + 2k_{\text{b1}}\phi_{\text{r}} + 2k_{\text{d}}\phi_{\text{r}}$, $\phi_{\text{r}wc} = \frac{w_{\text{c}}}{r} = \phi_{\text{r4}} - \phi_{\text{r3}} - \phi_{\text{r1}} - k_{\text{d}}\phi_{\text{r}} - k_{\text{b1}}\phi_{\text{r}} - k_{\text{b2}}\phi_{\text{r}}$.

3.2.3. *Analytical method for optimal design of MR valves.*

3.2.3.1. Principle of optimization method with predefined threshold. Considering multiple design parameters with coupling effects, an optimization process should be conducted in the design of the MR valve. A multi-objective function is employed in the literature [22],

$$J_{\text{opt}} = \alpha_1\frac{\phi_{\text{DVMR}}}{\phi_{\text{DVMRref}}} + \alpha_2\frac{F_\tau}{F_{\tau\text{ref}}} + \alpha_3\frac{T_{\text{inref}}}{T_{\text{in}}} \tag{24}$$

where α_1, α_2, α_3 are factors for the weighted objective function. ϕ_{DVMRref}, $F_{\tau\text{ref}}$, T_{inref} are reference values that are selected from the current groups of design sets.

However, the weight factors in equation (24) are often empirically specified and have no systematic method for selection. As a result, different configuration of weight factors will lead to significantly different damping capability and consequently great impact on the achievable performance in semi-active vibration control. Thereafter, an analytical optimization method with predefined threshold (e.g. minimum performance requirements) for the MR valve design is proposed. Importantly, the proposed method can maximize achievable pressure drop (which is proportional to active damping force) and simultaneously fulfil minimum requirements corresponding to predefined thresholds in terms of reference passive damping ratio and time constant with some internal design variables to be optimized under practical constraints for guaranteeing high efficiency. This method could avoid empirical methods or uncertainty in weight selection procedure in multi-objective optimization and guarantees fairly small damping ratio and time constant as expected. The principle of the proposed optimization method with predefined threshold is illustrated as follows.

Considering the structure of the MR valve in figure 10, the available magnetic flux density under applied current is constrained by four critical section areas, i.e.

$$A_{11} = 2\pi R_{\text{c}}L_{\text{a}}, \tag{25a}$$

$$A_9 = \pi[R^2 - (R - t_h)^2], \tag{25b}$$

$$A_4 = \pi R_{\text{c}}^2, \tag{25c}$$

$$A_{\text{MR}} = 2\pi\bar{R}_{\text{d}}L_{\text{a}}. \tag{25d}$$

According to Gauss's law, the magnetic flux conservation rule of the circuit in the critical section area is given by [23]

$$\Phi = B_{11}A_{11} = B_9A_9 = B_4A_4 = B_{\text{MR}}A_{\text{MR}}. \tag{26}$$

Combining equations (25) and (26), one obtains,

$$B_{11}2\pi R_{\text{c}}L_{\text{a}} = B_9[R^2 - (R - t_h)^2] = B_4\pi R_{\text{c}}^2 = B_{\text{MR}}2\pi\bar{R}_{\text{d}}L_{\text{a}}. \tag{27}$$

The active length ratio ϕ_{La} would be tentatively synthesized in terms of specified variables considering practical constraints such as saturation constraint of magnetic material and MR fluid, predefined threshold, and high efficient usage of geometric volume etc. Then the optimal ϕ_{La} and other internal design variables (gap size ratio, outer housing ratio and valve core ratio) could be specified for maximizing pressure drop of the MR valve.

Step 1: Calculate the valve core ratio by assuming that $B_4 = B_9 > B_{11}$ in equation (27), which is given by

$$\phi_{\text{r1}} = \sqrt{(2\phi_{\text{r4}} - \phi_{\text{r3}})\phi_{\text{r3}}} \qquad \text{and} \qquad \phi_{\text{La}} \geq 0.5\phi_{\text{r1}}. \tag{28}$$

Step 2: Derive the permissible value of ϕ_{La} according to practical constraints.

On the one hand, ϕ_{La} is constrained by magnetic saturation of the magnetic material used in the MR valve. Thus

$$B_{11} = \frac{B_{\text{MR}}2\pi\bar{R}_{\text{d}}L_{\text{a}}}{2\pi R_{\text{c}}L_{\text{a}}} = \frac{\mu_0\mu_{\text{MR}}\phi_{\text{r}Rd}}{\phi_{\text{r1}}} \times \left[\frac{Ir}{2A_w}(\Delta_{\text{H1}} - \Delta_{\text{H2}}\phi_{\text{La}}) + H_{\text{MR0}}\right] \leq B_{\text{sat}}, \tag{29a}$$

$$B_4 = \frac{B_{\text{MR}}2\pi\bar{R}_{\text{d}}L_{\text{a}}}{\pi R_{\text{c}}^2} = \frac{2\mu_0\mu_{\text{MR}}\phi_{\text{r}Rd}}{\phi_{\text{r1}}^2} \times \left[\frac{Ir}{2A_w}(\Delta_{\text{H1}} - \Delta_{\text{H2}}\phi_{\text{La}}) + H_{\text{MR0}}\right]\phi_{\text{La}} \leq B_{\text{sat}}, \tag{29b}$$

Table 2. Default value of non-dimensional design parameters.

Parameter	Value	Parameter	Value	Parameter	Value	Parameter	Value	Parameter	Value
ϕ_{E1}	1.447×10^{-6}	ϕ_{r4}	2	k_{b1}	1	r_0 (mm)	13.856	T_{inref} (s)	0.025
ϕ_{M1}	1.1052	ϕ_{LP}	2.3	k_{b2}	1	ϕ_{gr}	1		
ϕ_{M2}	4.7288	ϕ_p	277.13	k_d	3	ξ_{ref}	0.035		

$$B_9 = \frac{B_{MR} 2\pi \bar{R}_d L_a}{\pi[R^2 - (R - t_h)^2]} = \frac{2\phi_{rRd}}{2\phi_{r4}\phi_{r3} - \phi_{r3}^2} \mu_0 \mu_{MR} \times \left[\frac{Ir}{2A_w}(\Delta_{H1} - \Delta_{H2}\phi_{La}) + H_{MR0}\right]\phi_{La} \le B_{sat}. \quad (29c)$$

In addition, the applied magnetic field intensity should not be too large to prevent MR fluids from operating in a saturated yield stress. The latter can result in less sensitivity in control.

$$0 < H_{MR} = \frac{Ir}{2A_w}(\Delta_{H1} - \Delta_{H2}\phi_{La}) \le H_{MRsat}. \quad (29d)$$

Combining equations (28) and (29), the active length ratio ϕ_{La} should satisfy the following expressions

$$\begin{aligned}
&\phi_{La} \ge \frac{\Delta_1[\Delta_{H1} + \Delta_{M1}] - \Delta_{M2}}{\Delta_1 \Delta_{H2}} \\
&\phi_{La} \ge \frac{\Delta_2(\Delta_{H1} + \Delta_{M1}) + \sqrt{\Delta L_2}}{2\Delta_2 \Delta_{H2}} \quad \text{or} \\
&\quad \phi_{La} \le \frac{\Delta_2(\Delta_{H1} + \Delta_{M1}) - \sqrt{\Delta L_2}}{2\Delta_2 \Delta_{H2}} \\
&\phi_{La} \ge \frac{\Delta_3(\Delta_{H1} + \Delta_{M1}) + \sqrt{\Delta L_3}}{2\Delta_3 \Delta_{H2}} \quad \text{or} \\
&\quad \phi_{La} \le \frac{\Delta_3(\Delta_{H1} + \Delta_{M1}) - \sqrt{\Delta L_3}}{2\Delta_3 \Delta_{H2}} \\
&\frac{\Delta_{H1} + \Delta_{M1} - \Delta_{M4}}{\Delta_{H2}} \ge \phi_{La} \ge \frac{\Delta_{H1} + \Delta_{M1} - \Delta_{M3}}{\Delta_{H2}} \\
&\phi_{La} \ge 0.5\phi_{r1}
\end{aligned} \quad (30)$$

where $\Delta_1 = \frac{\phi_{rRd}}{\phi_{r1}}$, $\Delta_2 = \frac{2\phi_{rRd}}{\phi_{r1}^2}$, $\Delta_3 = \frac{2\phi_{rRd}}{2\phi_{r4}\phi_{r3} - \phi_{r3}^2}$, $\Delta_{M1} = \frac{H_{MR0}}{H_{MRsat}}\phi_{M2}\frac{1}{\phi_{gr}}$, $\Delta_{M2} = \phi_{M1}\phi_{M2}\frac{1}{\phi_{gr}}$, $\Delta_{M3} = \phi_{M2}\frac{1}{\phi_{gr}}$, $\Delta_{M4} = \frac{H_{MR\,min}}{H_{MRsat}}\phi_{M2}\frac{1}{\phi_{gr}}$, $\Delta L_2 = \Delta_2^2(\Delta_{H1} + \Delta_{M1})^2 - 4\Delta_2\Delta_{H2}\Delta_{M2}$, $\Delta L_3 = \Delta_3^2(\Delta_{H1} + \Delta_{M1})^2 - 4\Delta_3\Delta_{H2}\Delta_{M2}$. (If ΔL_2 or ΔL_3 has a negative value, the corresponding inequalities are always satisfied.)

On the other hand, several predefined thresholds (e.g. small passive damping ratio and time constant) are added to the optimization process in order to achieve better performance in vibration control without uncertainty in the weight selection procedure. The constraints for non-dimensional variables ξ_2 and ϕ_{Tin} are given by

$$\xi_2 = 12\pi n(\Delta_{p1}\phi_{La} + \Delta_{p2})\frac{\phi_{Apd}}{\phi_r^2}\phi_{E1}\phi_{gr} \le \xi_{ref} \quad (31a)$$

$$\phi_{Tin} = \frac{T_{in}}{r_0^2/r_{w1}} = \Delta_5[(\Delta_{H1} + \Delta_{M1})\phi_{La} - \Delta_{H2}\phi_{La}^2] \times \phi_{gr}^2 \le \phi_{Tinref}. \quad (31b)$$

Therefore, the solution of ϕ_{La} is given by

$$\begin{aligned}
&\phi_{La} \le \frac{1}{\Delta_{p1}}\left[\frac{\xi_{ref}\phi_r^2}{12\pi n\phi_{E1}\phi_{Apd}} - \Delta_{p2}\right] \\
&\phi_{La} \ge \frac{\Delta_4\Delta_5(\Delta_{H1} + \Delta_{M1}) + \sqrt{\Delta L_7}}{2\Delta_4\Delta_5\Delta_{H2}} \quad \text{or} \\
&\quad \phi_{La} \le \frac{\Delta_4\Delta_5(\Delta_{H1} + \Delta_{M1}) - \sqrt{\Delta L_7}}{2\Delta_4\Delta_5\Delta_{H2}}
\end{aligned} \quad (32)$$

where $\Delta L_7 = \Delta_5^2(\Delta_{H4} + \Delta_{M1})^2 - 4\Delta_5\Delta_{H2}\phi_{Tinref}$, $\Delta_4 = \phi_{gr}^2$.

Combining equations (30) and (32), the available range of ϕ_{La} could be specified and the achievable damper performance calculated according to equation (23) with an appropriate ϕ_{La} for maximizing active pressure drop within its available range.

In summary, the design procedure is given as follows.

(1) Specify the reference radius of the MR damper cylinder r_0, required reference passive damping ratio ξ_{ref} and non-dimensional time constant ϕ_{Tinref} according to the system level design. Select a type of MR fluid.
(2) Specify external design variables including geometric variables ϕ_{r4}, ϕ_{LP}, k_d, k_{b1}, k_{b2}, ϕ_{pt}, material parameters ϕ_{M1} and excitation variable ϕ_{M2}, ϕ_{E1} as shown in table 1.
(3) Select initial values for two internal design variables ϕ_r and ϕ_{r3}.
(4) Follow *steps 1–2* above to calculate the permissible non-dimensional active length ratio ϕ_{La} according to equations (30) and (32). If there are any invalid values in the calculation (such as negative value for geometry size), repeat (3) and (4) through choosing other values of internal design variables.
(5) Calculate achievable pressure drop with equation (23) through substituting ϕ_{La} obtained from (4).
(6) Increase the values of the non-dimensional variables ϕ_r and ϕ_{r3}, repeat (3)–(5) until the maximum active damping force is found.

3.2.4. Optimization results. Default values for some design parameters are used as shown in table 2 according to practical constraints and a sensitivity analysis for the MR valve with these external design parameters using the analytical non-dimensional models developed above.

Figure 11 shows the achievable performance with respect to different values of ϕ_{LP} and ϕ_{r4} using the proposed optimization method with predefined threshold. It can be seen from figure 11 that the achievable passive damping ratio and time constant are always less than reference values as expected, no matter what design parameters are chosen. That is, the small passive damping ratio and time constant could be guaranteed for achieving satisfactory isolation performance at high frequency and good dynamic response, and at the same

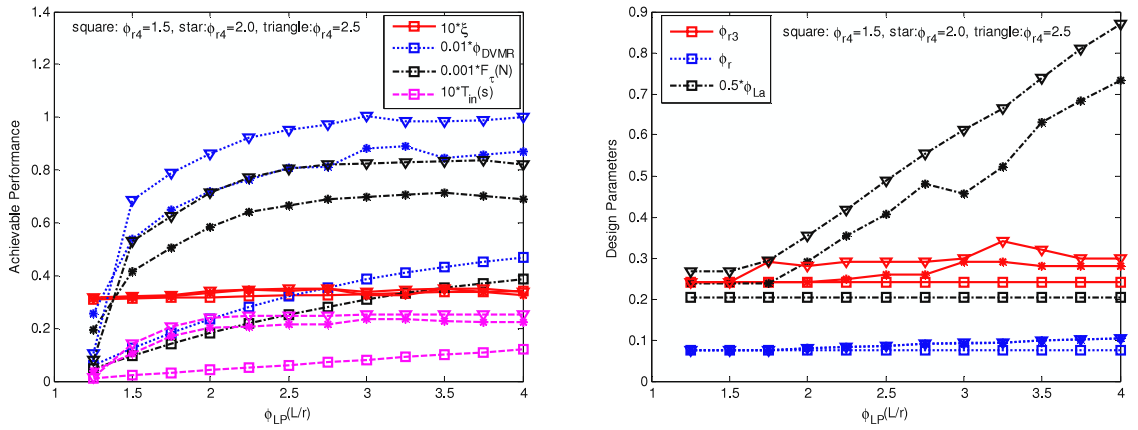

Figure 11. (a) The achievable performance and (b) optimized geometric parameters of the MR valve with respect to ϕ_{LP} and ϕ_{r4}.

Table 3. Practical realization for the actual plant system. (Note: P_s is the relative pressure of the source supply. L_{u0}, L_{d0} and L_{c0} are the effective initial length of the upper, lower and auxiliary pneumatic chambers, respectively, $\Delta p(\phi_L)$ is the maximum variation of operational pressure variation dependent on ϕ_L seen from figure 5. I_{max} is the required applied current, B_s is the minimum saturation magnetic flux density.)

Preliminary parameter setting	Involved non-dimensional parameters	Transformation from the non-dimensional to the practical parameters
$\hat{x}_{b0}$, m_0, P_s	$\phi_L \geq 3$, $\xi_3 \approx 0.25$, $0 \leq \phi_{P01} \leq 4$, $0 \leq \phi_{V01} \leq$ 4–5	$L_0 = L_{u0} = L_{d0} = L_{c0} = \phi_L \hat{x}_{b0}$, $P_{d0} = \frac{P_s + P_{atm}}{\Delta p(\phi_L)} \frac{1}{\phi_{P01}}$, $A_d \geq \frac{m_r g - s_u P_{atm} A_u}{P_{dr} - P_{atm}}$, $\omega_{n0} \approx \sqrt{\frac{\kappa g}{L_0}}$
AWG of coil wire, MR fluid	$\phi_{r4} =$ 1.5–2.5, $\phi_{LP} =$ 1.5–2.5	$r = \phi_{gr} r_0$, $R = r\phi_{r4}$, $L = r\phi_{LP}$, $r_t = (\frac{L_t r^3}{\phi_{pf}})^{1/4}$, $I_{max} = 2A_w H_{MRsat}/(r_0 \phi_{M2})$, $B_s = \phi_{M1} \mu_0 \mu_{MR} H_{MRsat}$

time the active damping force is maximized for effectively reducing the resonance peak through employing the proposed optimization method with predefined threshold for the MR valve. It should be noted that when ξ_{ref} is set too small, the achievable active force will become small although the dynamic range may be large, which is not beneficial for effective resonance attenuation. Furthermore, it is noted from figure 11 that there is no solution for some design parameters (e.g. $\phi_{LP} < 1$) due to the constraint of predefined threshold in optimization. It is obviously noticeable that the achievable dynamic range and active damping force are increased dramatically within $\phi_{LP} =$ 1–1.5 and gradually increased within $\phi_{LP} =$ 1.5–2.5, and then slightly increased at $\phi_{LP} > 2.5$, which indicates that the appropriate total length of MR valve for compact volume design could be obtained at $\phi_{LP} =$ 1.5–2.5. On the other hand, the achievable performance with total width of MR valve justified by ϕ_{r4} exhibits similar characteristics to ϕ_{LP}. The achievable performance is greatly enhanced within $\phi_{r4} =$ 1.5–2 and slowly changed with $\phi_{r4} >$ 2.5, which indicates that the appropriate value for width ratio ϕ_{r4} is about $\phi_{r4} =$ 1.5–2.5. The other design parameters upon achievable performance can be analyzed in a similar way. Therefore, the proposed optimization method with predefined threshold based on non-dimensional analytical formulations for component level design of MR valves in the MrEPI removes the difficulty in empirically selecting appropriate weight in conventional optimization methods and facilitates sensitivity analysis in synthesizing appropriate design parameters so that the entire optimization process of the MR valve is more systematic and efficient.

3.3. Practical realization

The optimal values for the non-dimensional parameters obtained above should be transformed into practical parameters for realization based on practical application requirements. To illustrate this, the preliminary parameter setting, the involved non-dimensional parameters from system level design and component level design, and the transformation from non-dimensional parameters to practical ones are shown in table 3.

4. Achievable isolation performance for the optimally designed MrEPI

The isolation performance for the optimized MrEPI ($\xi_2 =$ 0.033, $\phi_{DVMR} =$ 78.5) with independently adjustable stiffness and damping is evaluated. For the MrEPI, its stiffness could be firstly adjusted at an appropriate value according to specific application requirement through regulation of additional pressure ratio or additional volume ratio by pneumatic on–off valves, and then the active damping under such a setting stiffness is only controlled by the MR valve with appropriate semi-active controllers in order to attenuate the resonance peak over a broad frequency band [1].

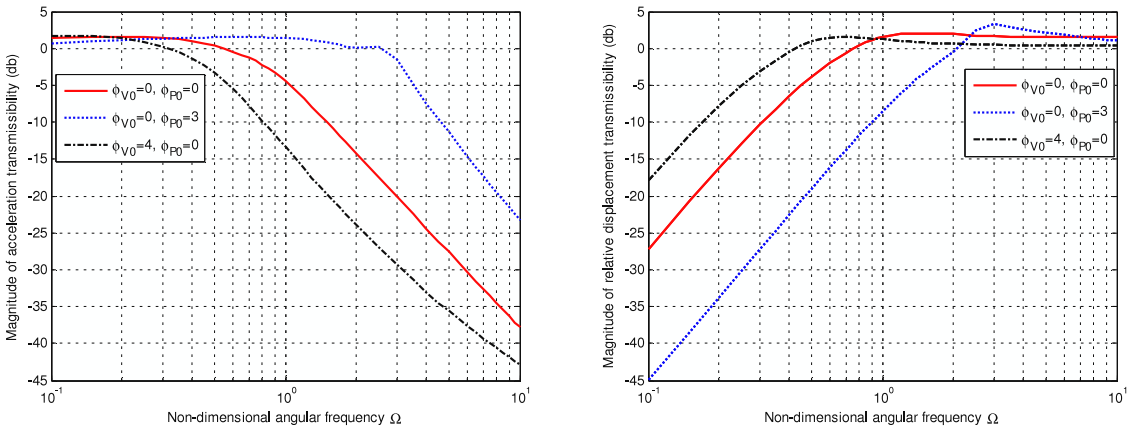

Figure 12. The isolation performance of the MrEPI with different stiffness levels dependent on ϕ_{P0} or ϕ_{V0}.

Figure 12 shows the isolation performance of the MrEPI (acceleration transmissibility and relative displacement) under different stiffness levels dependent on additional pressure ratio ϕ_{P01} or additional volume ratio ϕ_{V01} ($0 \leq \phi_{P01} \leq 3$, $0 \leq \phi_{V01} \leq 4$) using a semi-active sky-hook controller for the MR damper as in [30]. The theoretical stiffness adjustment could be calculated from $K_{\text{equ}} = 1/6$ ($\phi_{V01} = 4$) to $K_{\text{equ}} = 5$ ($\phi_{P01} = 3$) according to equation (10), and could be verified by the natural frequency seen from figure 12. It can be seen from figure 12 that excellent isolation performance with effective resonance attenuation and fast mitigation at high frequency under both low and high stiffness can be achieved, because a fairly small passive damping ratio can be guaranteed and a larger active damping force can be optimized for the MrEPI. Therefore, the proposed optimization method with predefined threshold achieves excellent isolation performance with a systematic parameter selection procedure and clear insight into the achievable performance compared with existing methods [22] which employ a weight selection procedure by trial to cope with the underlying multiple-objective optimization problem.

5. Conclusions

A systematic and effective non-dimensional analytical model based optimization method for the analysis and design of a class of nonlinear vibration isolator systems using pneumatic springs and MR dampers such as the typical MrEPI is developed with the consideration of practical constraints and high efficiency. The design procedure is to find the best geometry dimension, material properties and exciting conditions (see table 1) of the isolator system for maximizing adjustable stiffness and damping as well as facilitating vibration control of the isolator. This is achieved by analyzing the sensitivity of design parameters upon the achievable performance irrespective of bulky or small system mass configuration. The design is accomplished through three levels: system level design for pneumatic spring and MR damper elements, component level design for the MR valve and practical realization design for real plant systems. As a summary, the following points can be concluded.

(1) The system level design involves synthesizing non-dimensional parameters including nonlinear ratio, pressure ratio and volume ratio of the pneumatic spring, as well as passive and dynamic ranges of MR damping for maximizing the adjustable range of achievable performance and minimizing volume usage for compact and efficient considerations.

(2) The component level design involves an analytical method for optimal design of the MR valve with integrated non-dimensional variables including both geometric and electromagnetic circuits through introducing a multi-objective function with predefined threshold of passive damping ratio and time constant, which guarantees a minimum requirement of isolation performance of the MrEPI with a systematic optimization process and is exempted from empirical trials and uncertainty in weight selection.

(3) The practical realization design for a real plant system is conducted according to practical application requirements so that the entire design procedure is accomplished from the non-dimensional model based analysis and optimization.

(4) The isolation performance of the optimal MrEPI under harmonic disturbances is investigated using a semi-active sky-hook controller for the MR damper under certain stiffness settings realized by pressure/volume regulation of the pneumatic chamber. The simulation results demonstrated that excellent vibration isolation performance (e.g. effective resonance attenuation and fast energy mitigation at high frequency for acceleration and relative displacement transmissibility irrespective of low or high stiffness configuration) could be achieved with the optimized MrEPI compared to some existing systems using only pneumatic or only MR fluid elements.

Acknowledgments

The authors would like to gratefully acknowledge the support from a GRF project (Ref 517810) of Hong Kong RGC, Department General Research Funds and Competitive Research Grants of Hong Kong Polytechnic University.

Appendix

Table A.1. Default values and illustrations of non-dimensional variables for the MrEPI.

Variable	Name	Definition	Illustration
ϕ_{L}	Nonlinear ratio	$\phi_{\mathrm{L}} = \frac{L_0}{\hat{x}_{\mathrm{b0}}}$	Ratio of reference initial length of pneumatic spring to maximum excitation amplitude, which depicts a nonlinearity degree of the system
ϕ_{P0}	Additional pressure ratio	$\phi_{\mathrm{p0}} = \frac{\Delta P_{\mathrm{d}}}{P_{\mathrm{d}r}}$	Ratio of additional initial pressure to reference pressure, which depicts the adjustable stiffness incurred by variation of cylinder pressure
ϕ_{V0}	Additional volume ratio	$\phi_{V0} = \frac{\Delta V_{\mathrm{d}}}{V_{\mathrm{d}r}}$	Ratio of additional initial volume to reference volume, which depicts the adjustable stiffness incurred by variation of cylinder volume
ϕ_{KP}	Pressure ratio of dual-working-chamber pneumatic spring	$\phi_{KP} = \frac{P_{\mathrm{u0}}A_{\mathrm{u}}}{P_{\mathrm{d}r}A_{\mathrm{d}r}}$	Ratio of pressure of upper pneumatic chamber to reference pressure
ϕ_{KL}	Volume ratio of dual-working-chamber pneumatic spring	$\phi_{KL} = \frac{L_{\mathrm{u0}}}{L_{\mathrm{d0}}}$	Ratio of initial length of upper pneumatic chamber to reference length
ξ	Passive viscous damping	$\xi = \frac{c_{\mathrm{vis}}}{2\sqrt{mk_0}}$	Passive linear viscous damping
ϕ_{DVMR}	Dynamic range of MR active damping	$\phi_{\mathrm{DVMR}} = \frac{F_\tau}{F_\eta}$	Dynamic range of active damping due to field-controlled yield force of MR fluid, which depicts the controllable active damping incurred by applied current of the MR valve
$\phi_{\lambda\mathrm{a}}$	Hysteretic width coefficient	$\phi_{\lambda\mathrm{a}} = \frac{\lambda_{\mathrm{a}}}{\sqrt{mk_0}}$	Parameter to capture the displacement-dependent hysteresis width in MR damping model
$\phi_{\lambda\mathrm{b}}$	Hysteretic slope coefficient	$\phi_{\lambda\mathrm{b}} = \frac{\lambda_{\mathrm{b}}}{\sqrt{mk_0}}$	Parameter to capture the velocity-dependent hysteresis slope in the MR damping model

Table A.2. Illustrations of symbols for the MrEPI.

Symbol	Illustration	Symbol	Illustration
P	Absolute gas pressure (bar)	V	Gas volume (m^3)
A	Effective area of pneumatic chamber (m^2)	L	Length of pneumatic chamber (m)
m_0	Reference payload mass (kg)	L_0	Initial length of pneumatic spring (m)
k_0	Reference stiffness ($\mathrm{N\ m}^{-1}$)	κ	Polytropic exponent
$\hat{x}_{\mathrm{b0}}$	Displacement amplitude under sinusoidal excitation (m)	s_{u}	Switching flag with $s_{\mathrm{u}} = 0$ or $s_{\mathrm{u}} = 1$ for the case of a single-working-chamber and double-working-chamber pneumatic spring, respectively

Table A.3. Illustrations of subscript and prefix for symbols.

Subscript	Illustration	Subscript	Illustration
0	Static or initial value	n	Non-dimensional output
u	Upper chamber of pneumatic spring	b	Motion for base excitation
d	Low chamber of pneumatic spring	m	Motion for middle plate of an isolator
c	Auxiliary chamber of pneumatic spring	r	Reference state
Prefix	**Illustration**	**Prefix**	**Illustration**
Δ	Variation of variables	ϕ	Non-dimensional variable

References

[1] Deo H V and Suh N P 2005 Variable stiffness and variable ride-height suspension system and application to improved vehicle dynamics *2005 SAE World Congr. (Detroit, MI, April)*

[2] Bauer W 2011 *Hydropneumatic Suspension Systems* (Berlin: Springer)

[3] Guglielmino E, Sireteanu T, Stammers C W, Ghita G and Giuclea M 2008 *Semi-Active Suspension Control, Improved Vehicle Ride and Road Friendliness* 1st edn (London: Springer)

[4] Choi Y T and Wereley N M 2003 Vibration control of a landing gear system featuring electrorheological/magnetorheological fluids *J. Aircr.* **40** 432–9

[5] Erin C and Wilson B 1998 An improved model of a pneumatic vibration isolator: theory and experiment *J. Sound Vib.* **218** 81–101

[6] Yang G, Spencer B F, Carlson J D and Sain M K 2002 Large-scale MR fluid dampers modeling, and dynamic performance considerations *Eng. Struct.* **24** 309–23

[7] Liu Y, Matsuhisa H and Utsuno H 2008 Semi-active vibration isolation system with variable stiffness and damping control *J. Sound Vib.* **313** 16–28
[8] Dong X, Yu M, Liao C and Chen W 2009 Impact absorbing control of magneto-rheological variable stiffness and damping system *J. Sichuan Univ. (Engineering Science Edition)* **41** 187–92 (in Chinese)
[9] Tanner E T 2003 Combined shock and vibration isolation through the self-powered, semi-active control of a magnetorheological damper in parallel with an air spring *PhD Thesis* Virginia Polytechnic Institute and State, USA
[10] Plooy N F, Heyns P S and Brennan M J 2005 The development of a tunable vibration absorbing isolator *Int. J. Mech. Sci.* **47** 983–97
[11] Anusonti-Inthra P 2002 Semi-active control of helicopter vibration using controllable stiffness and damping devices *PhD Thesis* The Pennsylvania State University, USA
[12] Zhu X C, Jing X J and Cheng L 2010 A magnetorheological fluid embedded pneumatic vibration isolator allowing independently adjustable stiffness and damping *Smart Mater. Struct.* **20** 085025
[13] Holtz M W and van Niekerk J L 2010 Modelling and design of a novel air-spring for a suspension seat *J. Sound Vib.* **329** 4354–66
[14] Quaglia G and Sorli M 2001 Air suspension dimensionless analysis and design procedure *Veh. Syst. Des.* **35** 443–75
[15] Lee J H and Kim K J 2009 A method of transmissibility design for dual-chamber pneumatic vibration isolator *J. Sound Vib.* **323** 67–92
[16] Moon J H and Lee B G 2010 Modeling and sensitivity analysis of a pneumatic vibration isolation system with two air chambers *Mech. Mach. Theory* **45** 1828–50
[17] Maciejewski I, Kiczkowiak T and Krzyzynski T 2009 Optimisation of pneumatic circuit aimed at improving the vibro-isolation properties of seat suspension *Proc. Appl. Math. Mech.* **9** 639–40
[18] Gavin H, Hoagg J and Dobossy M 2001 Optimal design of MR dampers *Proc. US–Japan Workshop on Smart Structures for Improved Seismic Performance in Urban Regions (Seattle WA, Aug.)* pp 225–36
[19] Nguyen Q H, Han Y M, Choi S B and Wereley N M 2007 Geometry optimization of MR valves constrained in a specific volume using the finite element method *Smart Mater. Struct.* **16** 2242–52
[20] Nguyen Q H, Choi S B and Wereley N M 2008 Optimal design of magnetorheological valves via a finite element method considering control energy and a time constant *Smart Mater. Struct.* **17** 025024
[21] Nguyen Q H and Choi S B 2009 Optimal design of MR shock absorber and application to vehicle suspension *Smart Mater. Struct.* **18** 035012
[22] Nguyen Q H and Choi S B 2009 Optimal design of a vehicle magnetorheological damper considering the damping force and dynamic range *Smart Mater. Struct.* **18** 015013
[23] Nguyen Q H, Choi S B, Lee Y S and Han M S 2009 An analytical method for optimal design of MR valve structures *Smart Mater. Struct.* **18** 095032
[24] Sathianarayanan D, Karunamoorthy L, Srinivasan J, Kandasami G S and Palanikumar K 2008 Chatter suppression in boring operation using magnetorheological fluid damper *Mater. Manuf. Process.* **23** 329–35
[25] Rosenfeld N C and Wereley N M 2004 Volume-constrained optimization of magnetorheological and electrorheological valves and dampers *Smart Mater. Struct.* **13** 1303–13
[26] Hiemenz G J, Hu W and Wereley N M 2008 Semi-active magnetorheological helicopter crew seat suspension for vibration isolation *J. Aircr.* **45** 945–53
[27] Liu Y, Waters T P and Brennan M J 2005 A comparison of semi-active damping control strategies for vibration isolation of harmonic disturbances *J. Sound Vib.* **280** 21–39
[28] Pang L, Kamath G M and Wereley N M 1998 Analysis and testing of a linear stroke magnetorheological damper *AIAA/ASME/AHS Adaptive Structures Forum* vol CP9803 *(Long Beach, CA, April)* pp 2841–2856, Part 4
[29] Wang D H and Liao W H 2011 Magnetorheological fluid dampers: a review of parametric modeling *Smart Mater. Struct.* **20** 023001
[30] Choi Y T and Wereley N M 2005 Mitigation of biodynamic response to vibratory and blast-induced shock loads using magnetorheological seat suspensions *Proc. Inst. Mech. Eng.* D **219** 741–53
[31] Weber F and Boston C 2011 Clipped viscous damping with negative stiffness for semi-active cable damping *Smart Mater. Struct.* **20** 045007